IEEE Access
Multidisciplinary | Rapid Review | Open Access Journal

Received 3 June 2023, accepted 12 June 2023, date of publication 20 June 2023, date of current version 28 July 2023.

Digital Object Identifier 10.1109/ACCESS.2023.3287931

RESEARCH ARTICLE

Slotted Aloha With Capture for OWC-Based IoT: Finite Block-Length Performance Analysis

TIJANA DEVAJA[1], (Graduate Student Member, IEEE), MILICA PETKOVIĆ[1], (Member, IEEE), FRANCISCO J. ESCRIBANO[2], (Senior Member, IEEE), ČEDOMIR STEFANOVIĆ[3], (Senior Member, IEEE), AND DEJAN VUKOBRATOVIĆ[1], (Senior Member, IEEE)

[1]Faculty of Technical Sciences, University of Novi Sad, 21000 Novi Sad, Serbia
[2]Universidad de Alcalá, 28801 Alcalá de Henares, Spain
[3]Aalborg University, 2450 Aalborg, Denmark

Corresponding author: Tijana Devaja (tijana.devaja@uns.ac.rs)

This work was supported in part by the European Union Horizon 2020 Research and Innovation Program under Grant 856967, in part by the Secretariat for Higher Education and Scientific Research of the Autonomous Province of Vojvodina through the Project "Visible Light Technologies for Indoor Sensing, Localization and Communication in Smart Buildings" under Grant 142-451-2686/2021, and in part by the European Cooperation in Science and Technology (COST) Action through COST under Grant NEWFOCUS CA19111.

ABSTRACT In this paper, we analyze the throughput and reliability of an indoor optical wireless communication (OWC)-based Internet of Things (IoT) system based on Slotted ALOHA (SA) where IoT devices exchange data with an access point (AP). Assuming that the OWC receiver at the AP exploits the capture effect, we derive the error probability of decoding a short-length data packet that originates from a randomly selected OWC IoT device in the presence of interfering users. The analysis is based on the derivation of the signal-to-interference-plus-noise-ratio (SINR) statistics and the application of the finite block-length (FBL) information theory. Using these analytical results, we derive relevant performance parameters such as the system throughput and reliability expressed in terms of the outage probability of a user transmission. The main trade-offs between the system performance and the OWC system setup parameters are investigated, in particular, by stressing how the indoor OWC-based system geometry plays an important role in the system performance.Using extensive numerical results, we clearly describe how the presented results are used to optimize the SA-based indoor OWC IoT system design.

INDEX TERMS Finite block-length, error probability, Internet of Things, optical wireless communications, random access, slotted ALOHA, throughput.

I. INTRODUCTION

Optical wireless communications (OWC) have been recently gaining attention as a technology able to offload traffic from wireless radio-frequency (RF) technologies in indoor environments. This may alleviate the challenges posed by the spectrum crunch that affects the most intensively exploited bands. In fact, the RF spectrum shortage is continuously pushing for the opening of higher frequency bands for wireless communications, ranging from millimeter-wave, over terahertz to optical (infrared (IR) or visible) bands [1], [2], [3], [4]. Each of these possibilities target specific environments and applications, and the ongoing research points towards a combination of access strategies to meet the ever-increasing Internet of Things (IoT) requirements and the associated demand for resources.

In any case, using a specific frequency band for an IoT application is only a part of a wider context. Specifically, in a wireless IoT framework, where the communication medium is shared, granting a fair access to the shared resources and guaranteeing the link quality in presence of possible interference is of paramount importance [5], [6], while the sporadic nature of the IoT traffic and the short lengths of the exchanged data packets pose specific challenges in this

The associate editor coordinating the review of this manuscript and approving it for publication was Jose Saldana.

TABLE 1. List of symbols and notations.

Symbol	Name/explanation	Symbol	Name/explanation	Symbol	Name/explanation
$\mathbb{E}[\cdot]$	Mathematical expectation	$\mathbb{P}[\cdot]$	Probability of the event	$Q^{-1}(\cdot)$	Inverse Gaussian Q-function
U	Total number of IoT devices	U_a	Number of active users	$\mathcal{U}_a$	Set of active users in a slot
p_a	Activation probability	$\mathcal{B}$	Binomial distribution	u_i	Individual active users
$y(\cdot)$	Received signal	P_t	Transmitted optical power	$x(\cdot)$	Unit-power signal waveform
η	O/E conversion coefficient	h	Optical channel gain	$n(\cdot)$	Additive white Gaussian noise
$f_{r_i}(r)$	PDF of radial distance r_i	$f_{h_i}(h)$	PDF of optical channel gain h_i	$f_{\gamma_i}(\gamma)$	PDF of i-th user SINR
$F_{\gamma_i}(\gamma)$	CDF of i-th user SINR	$\varphi_{\gamma_i}(t)$	CF of i-th user SINR	$\Gamma(\cdot,\cdot)$	Upper incomplete gamma func.
$f_{\gamma_1}(\gamma)$	PDF of reference user SINR	$\varphi_{\gamma_1}(t)$	CF of reference user SINR	$f_{\mathrm{SINR}}(\gamma)$	PDF of SINR conditioned on U_a
A_r	Photodetector surface area	R_r	Responsivity	D	Radius
T_s	Optical filter gain	m	Lambertian order	ζ	Refractive index of lens at a PD
Ψ	FoV of receiver	$\Phi_{1/2}$	Semi-angle at half illuminance	N_0	Noise power spectral density
B	System noise bandwidth	ϵ	Error probability	R	Code rate
n	Number of channel uses	γ	Signal-to-noise ratio (SNR)	C	Channel capacity
V	Channel dispersion	T	Throughput	P_{out}	Outage probability

regard. In this context, well designed random access (RA) protocols are instrumental to obtain a good performance in the access network [7], [8], [9], [10], [11], [12]. Along the last decades, there has been a general trend to embrace interference in wireless media in order to efficiently exploit the available, scarce spectrum resources (e.g. by using spread spectrum or MIMO spatial multiplexing techniques). In the domain of access schemes, the same principle is applied through exploitation of the capture effect, which frequently occurs in wireless communications and through which user data may be recovered in presence of concurrent transmissions. Under such scenarios, collision avoidance ceases to be one the basic design principles for successful RA protocols, because, in fact, promoting collisions may become beneficial. In this way, a simple slotted ALOHA (SA) solution in combination with the exploitation of the capture effect at the physical layer can achieve a favorable throughput performance [13], [14], [15].

The IoT deployment scenario considered in this paper assumes an indoor space comprising large and unobstructed areas (e.g., a warehouse or an open-plan office), where a large quantity of devices collect, process and send data to a number of access points. In such situation, the use of RF links could lead to an intolerable level of interference and a high probability of packet loss due to collisions. However, transmission technologies based on OWC can help to tackle these challenges, despite their limited coverage. In fact, by resorting to OWC links, the interference across walls is eliminated, and a small scale indoor cellular network could be designed to cover the whole space with a minimal coverage overlapping, thus maximizing the overall throughput.

OWC systems were studied in the recent literature as a potential indoor IoT solution in current and upcoming generations of mobile communication technologies [16], [17], [18], [19], [20], [21], [22], [23]. For the interested reader, a detailed state-of-the-art of the OWC for the IoT has been presented in [24], mostly focusing on four main IoT domains: Internet of Terrestrial Things (IoTT), Internet of underWater Things (IoWT), Internet of Biomedical Things (IoBT), and Internet of underGround Things (IoGT). Different uplink RA approaches with sporadic and varying device activity in OWC-based IoT systems were analyzed in [25], [26], [27], and [28]. Specifically, [25] analyzed the uplink of a multi-receiver OWC system in the context of a massive IoT application, where a coded SA approach with successive interference cancellation was adopted. In [26], Zhao et al. analyzed a multi-packet reception (MPR)-aided visible light communications (VLC) system and introduced a novel Quality of Service (QoS)-driven non-carrier sensing RA scheme. The same authors also proposed a novel SA algorithm with heterogeneous delay that guarantees the QoS in the context of the MPR VLC system [27]. An optical camera communication based on the ALOHA RA scheme was assessed in [28], where the access probability of each terminal was optimized in order to guarantee access fairness and system throughput rate maximization.

In this paper, we push the state-of-the-art by analyzing and optimizing a slotted ALOHA-based access scheme that takes into account an advanced modelling of the physical layer via (i) characterization of the signal-to-interference-plus-noise ratio (SINR) in the presence of interfering, randomly activated users and (ii) characterization of the impact of the finite-block length (FBL) effects. The obtained analytical framework allows the derivation of the probability that a user transmission is decoded in the presence of the rest of interfering users. Based on this, other performance metrics can be derived and the access scheme optimized. To the best of our knowledge, this is the first work that investigates the FBL effects in such an OWC environment. In particular, information theory has traditionally focused on data transmission reliability through noisy channels that may be achievable for channel coded data with large block lengths, but the fact is that, for IoT applications, we are usually dealing with short block-length transmissions. In this sense, the so-called FBL information theory [29] provides us with the appropriate tools to analyze what relates to error probability estimation and the corresponding maximum achievable rate under a given message length constraint.

The presented work is an extension of the initial study of the SINR statistics for an OWC-based IoT system with

capture effect presented in [30]. In this respect, the main novelty of the paper is the error probability analysis based on FBL theory, as well as the analysis of the overall system throughput and the reliability in terms of the outage probability. The FBL performance analysis for this kind of OWC-based IoT system represents the appropriate method to set the system parameters during the system design, with the aim to achieve an optimal performance of the RA protocol.

The contributions of the paper can be summarized as follows:

1) We analyse an architecture for future IoT based on short-range OWC technology and design an access scheme for an OWC-based IoT indoor network. We analyze the scheme in the terms of the SINR of the accessing users and evaluate its performance. The analysis builds up on our previous work [30], which is here complemented by the error and coding rate characterization, enabling an accurate modelling of the physical layer effects.

2) The error and the coding rate characterizations are based on the FBL performance analysis for OWC-based IoT systems that is exposed in the paper. Specifically, from the SINR statistics it is possible to derive the error probability affecting the captured data packets, protected by an appropriate channel code, thereby determining the system performance.

3) Building up on the physical layer characterization, the paper presents the analysis of the overall system throughput and the reliability in terms of the outage probability.

4) We use numerical results to provide guidelines for the optimal system design, by exploring the effects of the main OWC parameters on the system performance. These contributions are particularly important, as a real-world IoT network deployment requires not only that its physical parameters are appropriately set, but also that the access protocol is properly configured to achieve the optimal performance.

5) We provide the overall throughput comparison of the SA based OWC system with capture effect, and the SA system without capture effect, in the FBL regime. The results can be used to have insights into the behavior of the proposed system, i.e., in which manner the system parameters setup affects the effectiveness of a more complex SA scheme implementation.

The rest of the paper is structured as follows. In Section II, we review the system model and set the main hypothesis. In Section III, we derive the SINR statistics for the proposed setup. In Section IV, we analyze the error probability and channel coding rate based on the FBL regime approach, as well as the overall system throughput and the reliability in terms of the outage probability. In Section V, we present and discuss the numerical results and, finally, in Section VI, we close the paper with the main conclusions.

II. SA-BASED INDOOR OWC IoT: SYSTEM MODEL

The context of this work comprises a communication scenario in which a total of U IoT devices equipped with OWC transmitters contend to access a common OWC access point (AP). The transmitting devices are uniformly placed on a horizontal plane, while the OWC AP is located at the ceiling, at a fixed location (see Fig. 1). This setup corresponds to an open-plan office space with IoT devices placed on tables or other furniture. The SA protocol [9] is used for uplink transmissions. Each IoT device is active for transmission with probability p_a in every slot, independently of its activity in other slots and of the activity of other devices during the same slot period. In other words, we consider Bernoulli arrivals on user basis. If a user is active in a slot, it transmits a fixed-length packet with finite (short) block-length. We denote the set of active users in a slot by $\mathcal{U}_a$, and by $U_a = |\mathcal{U}_a|$ the corresponding number of active users, where $0 \leq U_a \leq U$. It is straightforward to show that U_a is a random, binomially distributed parameter $\mathcal{B}(U, p_a)$. Finally, with a slight misuse of notation, we denote the individual active users by $u_i \in \mathcal{U}_a$, $i = 1, \cdots, U_a$, where their indexing is assigned arbitrarily.

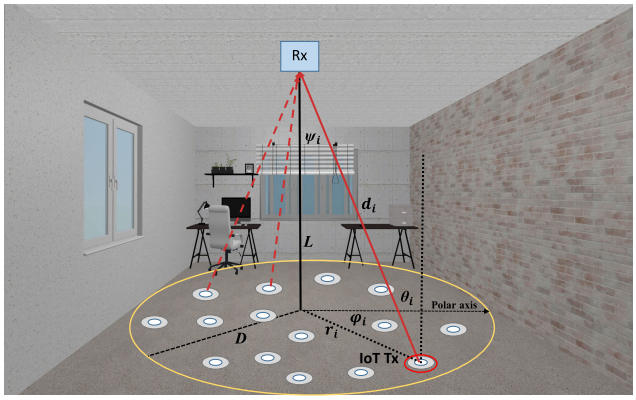

FIGURE 1. OWC-based indoor IoT system model.

The IoT devices use IR light emitted diode (LED) sources, and the physical transmission employs a simple intensity-modulation (IM) binary-format signaling (e.g., non-return-to-zero on-off keying (OOK)). All devices transmit with the same optical power regardless of any other condition. The OWC photo-detector (PD) receiver performs direct detection (DD) of the arriving light intensity [2]. The described OWC-based IoT architecture is simple, low cost and suitable for the low data rate requirements of short-range indoor IoT systems. It complements recently surveyed scenarios in [31], namely the VLC LED-based and the near-infrared laser-based ones, intended for high data rate connectivity and related applications. More specifically, our framework addresses the scenario envisaged by IEEE 802.15.7-2018 standard for short-range low-speed OWC IoT systems [19], within the proposed PHY II type architecture that uses IR signals with OOK format for both infrastructure (AP) and mobile (IoT user) devices.

At any given slot, the light intensity impinging the OWC PD receiver comprises the contribution of the U_a active users plus the background radiation noise. Assuming that the PD is working in a linear regime (which is a standard and a reasonable approximation in practical situations), the received signal after the conversion to the electrical domain (prior to

demodulation and decoding) can be modeled as

$$y(t) = \sum_{i=1}^{U_a} P_t \eta h_i x_i(t) + n(t), \tag{1}$$

where $x_i(t)$, $i = 1, \cdots, U_a$, is the unit-power signal waveform of the active user u_i, P_t is the transmitted optical power, η the optical-to-electrical conversion coefficient, $h_i \geq 0$ the optical channel gain from the user u_i to the AP, while $n(t)$ is an instance of additive white Gaussian noise (AWGN) with power spectral density $N_0/2$. This kind of noise process adequately models the distorting effects of the optical background radiation and the receiver thermal noise, and contributes to the overall signal-to-noise with a noise power $\sigma_n^2 = N_0 B$, where B is the system noise bandwidth.

Under these conditions, if a slot contains transmissions from two or more users (i.e., $U_a \geq 2$), the transmitted signals will not be recovered due to the collision in the observed slot. In that case, by exploiting the capture effect, the OWC AP receiver will attempt to decode the colliding transmissions, despite the presence of interfering users in the same slot. This contrasts the classical SA scheme, where the collision channel model is assumed.

When multiple users contend simultaneously for the same slot in SA, it is assumed by default that all transmitted signals in the slot fail to be received due to the collision. However, the capture effect may take place, that is, the strongest received signal may be successfully received despite the presence of interfering signals from other users in the same slot.[1]

We are interested in the probability that the receiver succeeds in decoding a randomly selected user among the set of active ones. For convenience, and without loss of generality, we assume that the index of such user (denoted as the *reference user* henceforth) corresponds to $i = 1$, i.e., u_1 is the reference user, while the rest of the active users u_i, $i = 2, \cdots, U_a$, are the interfering ones. Therefore, the received signal (1) can be rewritten as

$$y(t) = P_t \eta h_1 x_1(t) + \sum_{i=2}^{U_a} P_t \eta h_i x_i(t) + n(t), \tag{2}$$

where $x_1(t)$ is the signal waveform from the reference user u_1, $h_1 \geq 0$ is the corresponding optical channel gain, and the summation term represents the interference contribution from all other active users.

Based on (2), the SINR experienced by the reference user can be readily written as

$$SINR = \frac{P_t^2 \eta^2 h_1^2}{\sum_{i=2}^{U_a} P_t^2 \eta^2 h_i^2 + \sigma_n^2} = \frac{\gamma_1}{\sum_{i=2}^{U_a} \gamma_i + 1} = \frac{\gamma_1}{\gamma_I + 1}, \tag{3}$$

where

$$\gamma_1 = \frac{P_t^2 \eta^2 h_1^2}{\sigma_n^2}, \ \gamma_i = \frac{P_t^2 \eta^2 h_i^2}{\sigma_n^2}, \ \gamma_I = \sum_{i=2}^{U_a} \gamma_i. \tag{4}$$

The SINR depends not only on the number of active users, but also on the specific placements of the IoT devices with respect to the OWC AP (which, in turn, determines the specific values of the optical path gains, h_i). In the next section, we derive the statistics for the SINR observed by a randomly selected active user, based on the characteristics of the system setup and its optical parameters.

III. SINR STATISTICS FOR THE SA-BASED OWC IoT SYSTEM

As shown in Fig. 1, we assume that the devices are randomly and uniformly distributed over the same horizontal plane within an indoor circular coverage area of radius D. The OWC AP is positioned at a height L above the plane, over the center of the circle. The location of user u_i with respect to the OWC AP is determined by the angle θ_i (angle of irradiance), the angle φ_i, and the radius r_i in the polar coordinate plane. Furthermore, the corresponding angle of incidence into the AP is denoted as ψ_i, and the Euclidean distance between the corresponding LED transmitter and the PD receiver is denoted as d_i. The optical channel gain of the line-of-sight (LoS) link between u_i and the PD receiver can be determined as [32]

$$h_i = \frac{A_r \, (m+1) \, R_r}{2\pi d_i^2} \cos^m(\theta_i) \, T_s g(\psi_i) \cos(\psi_i), \tag{5}$$

where A_r is surface area of the PD, R_r is the responsivity, T_s is the gain of the optical filter, $g(\psi_i)$ is the response of the optical concentrator, and the factor m is described in the sequel. The optical concentrator is modeled as $g(\psi_i) = \zeta^2 / \sin^2(\Psi)$, for $0 \leq \psi_i \leq \Psi$, where ζ is the refractive index of the lens at the PD and Ψ denotes its field of view (FoV). Finally, the LED emission follows a generalized Lambertian radiation pattern with order $m = -\ln 2 / \ln\left(\cos \Phi_{1/2}\right)$, where $\Phi_{1/2}$ denotes the semi-angle at half illuminance[2] [2].

In this situation, if the surface of the PD receiver is parallel to the plane where the IoT devices are located, then $\theta_i = \psi_i$, $d_i = \sqrt{r_i^2 + L^2}$, $\cos(\theta_i) = \frac{L}{\sqrt{r_i^2 + L^2}}$, and equation (5) can be rewritten as

$$h_i = \frac{\mathcal{X}}{\left(r_i^2 + L^2\right)^{\frac{m+3}{2}}}, \tag{6}$$

where $\mathcal{X} = \frac{A_r (m+1) R_r}{2\pi} T_s g(\psi_i) \, L^{m+1}$ is a factor that does not depend on the specific placement of the IoT device, provided that the angle ψ_i lies below the PD FoV (a condition met for the values of D and L considered here, so that there would be no IoT devices excluded from the coverage area of the AP).

[1] The capture effect occurs if SINR of the target user is above a predefined threshold called capture ratio, whose value depends on the coding/modulation technique used in a particular system.

[2] We assume that all LEDs are characterized by the same parameters, i.e., $m_i = m$ and $\Phi_{1/2}^i = \Phi_{1/2} \ \forall i$.

As the IoT devices are uniformly distributed, the PDF of their radial distance r_i from the centre of the circle is [33]

$$f_{r_i}(r) = \frac{2r}{D^2}, \quad 0 \le r \le D. \tag{7}$$

By using expressions (6) and (7), and standard RV transformation techniques, the PDF of the optical channel gains, h_i, can be derived as

$$f_{h_i}(h) = \frac{2\mathcal{X}^{\frac{2}{m+3}}}{D^2(m+3)} h^{-\frac{m+5}{m+3}}, \quad h_{\min} \le h \le h_{\max}, \tag{8}$$

where $h_{\min} = \frac{\mathcal{X}}{(D^2+L^2)^{\frac{m+3}{2}}}$ and $h_{\max} = \frac{\mathcal{X}}{L^{m+3}}$.

The PDF of γ_i, defined in (4), can be similarly derived as [33]

$$f_{\gamma_i}(\gamma) = \frac{(\mu\mathcal{X}^2)^{\frac{1}{m+3}}}{D^2(m+3)} \gamma^{-\frac{m+4}{m+3}}, \quad \gamma_{\min} \le \gamma \le \gamma_{\max}, \tag{9}$$

where $\gamma_{\min} = \frac{\mu\mathcal{X}^2}{(D^2+L^2)^{m+3}}$, $\gamma_{\max} = \frac{\mu\mathcal{X}^2}{L^{2(m+3)}}$, and $\mu = \frac{P_t^2\eta^2}{\sigma_n^2}$.

The CDF of γ_i can be easily derived as

$$F_{\gamma_i}(\gamma) = \begin{cases} 1 + \dfrac{L^2 - (\mu\mathcal{X}^2/\gamma)^{\frac{1}{m+3}}}{R^2}, & \gamma_{\min} \le \gamma \le \gamma_{\max} \\ 1, & \gamma > \gamma_{\max} \end{cases}. \tag{10}$$

To get the statistical characterization of the overall SINR, we can use the characteristic function (CF) approach [34]. In this case, the CF of $\gamma_i = \frac{P_t^2\eta^2 h_i^2}{\sigma_n^2}$ can be derived via (9) as

$$\begin{aligned} &\varphi_{\gamma_i}(t) \\ &\triangleq \mathbb{E}\left[e^{jt\gamma_i}\right] = \int_{-\infty}^{\infty} e^{jtx} f_{\gamma_i}(\gamma)\, \mathrm{d}\gamma \\ &= \frac{(\mu\mathcal{X}^2)^{\frac{1}{m+3}}}{D^2(m+3)} \int_{\gamma_{\min}}^{\gamma_{\max}} \gamma^{-\frac{m+4}{m+3}} e^{jt\gamma}\, \mathrm{d}\gamma = \frac{(\mu\mathcal{X}^2)^{\frac{1}{m+3}}}{D^2(m+3)} \\ &\quad \times \left(\Gamma\left(-\frac{1}{m+3}, -jt\gamma_{min}\right) - \Gamma\left(-\frac{1}{m+3}, -jt\gamma_{max}\right)\right), \end{aligned} \tag{11}$$

where $\Gamma(s,z) = \int_z^{\infty} t^{s-1}e^{-t}\mathrm{d}t$ is the upper incomplete gamma function [35, (8.35)].

A. CONTRIBUTION TO THE SINR STATISTICS FROM THE REFERENCE USER

For the reference user, the PDF of γ_1 can be calculated as a particular case of equation (9), rewritten here for clarity

$$f_{\gamma_1}(\gamma) = \frac{(\mu\mathcal{X}^2)^{\frac{1}{m+3}}}{D^2(m+3)} \gamma^{-\frac{m+4}{m+3}}, \quad \gamma_{\min} \le \gamma \le \gamma_{\max}. \tag{12}$$

B. CONTRIBUTION TO THE SINR STATISTICS FROM THE INTERFERING USERS

The channel gains h_i (thus also γ_i) are independent and identically distributed (i.i.d.) RVs when the IoT device locations are also i.i.d. RVs. In this case, the CF of $\gamma_I = \sum_{i=2}^{U_a} \gamma_i$ can be determined as [34]

$$\begin{aligned} \varphi_{\gamma_I}(t) &\triangleq \mathbb{E}\left[e^{jt\gamma_I}\right] = \mathbb{E}\left[e^{jt\sum_{i=2}^{U_a}\gamma_i}\right] = \mathbb{E}\left[\prod_{i=2}^{U_a} e^{jt\gamma_i}\right] \\ &= \prod_{i=2}^{U_a} \mathbb{E}\left[e^{jt\gamma_i}\right] = \prod_{i=2}^{U_a} \varphi_{\gamma_i}(t) = \varphi_{\gamma_i}^{U_a-1}(t), \end{aligned} \tag{13}$$

where the CF of γ_i is defined in (11). The PDF of γ_I can be derived as

$$\begin{aligned} f_{\gamma_I}(\gamma) &= \frac{1}{2\pi}\int_{-\infty}^{\infty} e^{-jt\gamma}\varphi_{\gamma_I}(t)\, \mathrm{d}t \\ &= \frac{1}{2\pi}\int_{-\infty}^{\infty} e^{-jt\gamma}\varphi_{\gamma_i}^{U_a-1}(t)\, \mathrm{d}t, \end{aligned} \tag{14}$$

for $\gamma_{\min}^{U_a-1} \le \gamma \le \gamma_{\max}^{U_a-1}$.

C. OVERALL SINR STATISTICS FOR THE REFERENCE USER

As an intermediate step, we derive the PDF of the RV defined as $\lambda = \gamma_I + 1$, namely

$$\begin{aligned} f_{\lambda}(\lambda) &= \frac{f_{\gamma_I}(\gamma_I)}{|\frac{\mathrm{d}\lambda}{\mathrm{d}\gamma_I}|} = f_{\gamma_I}(\lambda - 1) \\ &= \frac{1}{2\pi}\int_{-\infty}^{\infty} e^{-jt(\lambda-1)}\varphi_{\gamma_i}^{U_a-1}(t)\, \mathrm{d}t, \end{aligned} \tag{15}$$

for $\gamma_{\min}^{U_a-1} + 1 \le \lambda \le \gamma_{\max}^{U_a-1} + 1$. Since γ_1 and γ_I are independent RVs, their joint PDF is $f_{\gamma_1,\lambda}(x,\lambda) = f_{\gamma_1}(x) f_{\lambda}(\lambda)$. The PDF of the SINR $= \frac{\gamma_1}{\lambda} = \frac{\gamma_1}{\gamma_I+1}$ of the reference user, conditioned on the total number of active users U_a, can be written as follows [36]

$$f_{SINR}(x|U_a) = \int_{-\infty}^{\infty} |\lambda| f_{\gamma_1}(x\lambda) f_{\lambda}(\lambda)\, \mathrm{d}\lambda, \tag{16}$$

where $f_{\gamma_1}(x)$ and $f_{\lambda}(\lambda)$ are defined in equations (12) and (15), respectively. After replacing (12) and (15) in equation (16), since $\lambda > 0$, this PDF can be written as

$$\begin{aligned} &f_{SINR}(x|U_a) \\ &= \frac{(\mu\mathcal{X}^2)^{\frac{1}{m+3}}}{2\pi D^2(m+3)} x^{-\frac{m+4}{m+3}} \\ &\quad \times \int_{\gamma_{\min}^{U_a-1}+1}^{\gamma_{\max}^{U_a-1}+1} \lambda^{-\frac{1}{m+3}} \left(\int_{-\infty}^{\infty} e^{-jt(\lambda-1)}\varphi_{\gamma_i}^{U_a-1}(t)\, \mathrm{d}t\right) \mathrm{d}\lambda, \end{aligned} \tag{17}$$

where $\varphi_{\gamma_i}(t)$ is the CF previously defined in equation (11).

Finally, the CDF of the SINR of the reference user, conditioned on the number of active users in the slot U_a, can be written as

$$F_{SINR}(\gamma|U_a) = \int_0^{\gamma} f_{SINR}(x|U_a)\, \mathrm{d}x. \tag{18}$$

This statistical characterization of the SINR will allow us to derive the error probability in the next section.

IV. PERFORMANCE ANALYSIS FOR THE OWC-BASED IoT SYSTEM BASED ON SA VIA THE FBL APPROACH

A. ERROR PROBABILITY FOR SA VIA THE FBL APPROACH

The theorem of Shannon-Hartley is developed under the hypothesis of infinite length data frames. In order to approach Shannon capacity, it is assumed that codes of asymptotically large block lengths are used. However, in typical IoT applications this assumption does not hold due to small IoT payloads whose size is of the order of hundreds of bits. For this reason, classical performance metrics such as the ergodic or outage capacity are not applicable for benchmarking the performance of IoT systems [37], [38]. For this reason, instead of the asymptotic information-theory results, in this work we apply the non-asymptotic, FBL performance bounds.

The basic goal of information theory is to quantify the extent to which reliable communication is possible over a noisy channel. A code of size N and block length n allows the communication of one of N messages via n uses of the channel. The fundamental trade-off between these quantities and the reliability of the communication process is captured by $N_\epsilon(n)$ − the largest size of the code with error probability ϵ (assuming equiprobable messages). A related, commonly used metric is the code rate $R = \log_2 N/n$. In this respect, investigating which is the maximum code rate $R_\epsilon(n)$ that allows a communication with n channel uses while providing reliability ϵ is the central question of FBL theory.

Building upon the classical Shannon's asymptotic results, Polyanskiy, Poor, and Verdu showed that for the AWGN channel with capacity $C(\gamma) = log_2(1+\gamma)$, where γ denotes the signal-to-noise ratio (SNR), the maximal achievable rate with decoding error probability ϵ can be tightly approximated as [29]

$$R = C(\gamma) - \sqrt{\frac{V_{AWGN}(\gamma)}{n}} Q^{-1}(\epsilon) + O\left(\frac{\log n}{n}\right), \quad (19)$$

where $Q^{-1}(\cdot)$ denotes the inverse of the Gaussian Q-function defined as $Q(z) = \int_z^\infty \frac{1}{\sqrt{2\pi}} e^{-\frac{t^2}{2}} dt$, while the so-called channel dispersion $V_{AWGN}(\gamma)$ is defined as

$$V_{AWGN}(\gamma) = \left(1 - \frac{1}{1+\gamma^2}\right) log_2^2(e). \quad (20)$$

In the context of this work, we are interested in the error probability of decoding a short-length data packet from a single active user by taking into account the interference contribution from all other active users in a given slot, see (3). Using the standard "treat interference as noise" approximation, one may initially consider the interference as an additional and independent Gaussian noise process. Strictly speaking, however, the aggregate interference does not obey Gaussian statistics (to achieve (19), transmitters need to use a non-Gaussian codebook), implying that the OWC receiver experiences non-Gaussian interference. A more precise and appropriate approximation is provided in [39], where non-Gaussian interference and nearest-neighbor decoding are assumed. In this case, the channel dispersion derived in [39] (see also [40]) should be applied, i.e.,

$$V(\gamma) = \frac{2\gamma}{1+\gamma} log_2^2(e), \quad (21)$$

instead of (20). On the other hand, for $n > 100$ channel uses, the term $O(\frac{\log n}{n})$ in (19) becomes negligible and can be omitted. Taking all this into account, the achievable rate could be tightly approximated as

$$R \approx C(\gamma) - \sqrt{\frac{V(\gamma)}{n}} Q^{-1}(\epsilon). \quad (22)$$

It is to be noted that the approximation (22) is established by characterizing the asymptotic behavior of analytically tractable achievability and converse bounds (see [29, Sec. III]).

For the system setup considered in this paper, relying on equation (22) and by setting $SINR = \gamma$ (which is dependent on the number of active users U_a), we can tightly approximate the decoding error probability as

$$\epsilon(\gamma, U_a) = Q\left(\sqrt{\frac{n}{V(\gamma(U_a))}} \left(C(\gamma(U_a)) - R\right)\right). \quad (23)$$

For the sake of clarity, in the previous equation we make the dependence of the error probability $\epsilon(\gamma, U_a)$ on the number of active users U_a explicit, although this dependence is implicit through the dependence of the SINR statistics $\gamma(U_a)$ on the number of active users U_a. By conditioning the error probability over the SINR, we get

$$\epsilon(U_a) = \int_\gamma \epsilon(\gamma, U_a) f_{SINR}(\gamma|U_a)\, d\gamma, \quad (24)$$

where $f_{SINR}(\gamma|U_a)$ was previously derived in (17). Finally, the unconditional error probability can be derived as

$$\epsilon = \sum_{k=1}^{U} \epsilon(U_a = k)\, \mathbb{P}[U_a = k], \quad (25)$$

where

$$\mathbb{P}[U_a = k] = \binom{U}{k} p_a^k (1-p_a)^{U-k}, \; k = 0, \cdots, U, \quad (26)$$

i.e., the number of active users U_a is a binomial random variable for the assumed Bernoulli arrival process.

B. THROUGHPUT FOR SA VIA THE FBL APPROACH

The overall system throughput is analysed as the parameter that describes the effective information transmission rate in the system. Based on the system throughput performance, it can be determined if the channel uses are effectively exploited, not only due to the effects of the noise but also due to the interference among randomly activated users.

Considering the FBL regime with a fixed code rate R, and the probability that the packet is decoded at each slot as

derived previously in (25), we define the throughput as

$$\begin{aligned} T &= 0 \cdot \mathbb{P}[U_a = 0] + \sum_{k=1}^{U} R \cdot (1 - \epsilon(U_a = k)) \cdot \mathbb{P}[U_a = k] \\ &= R \cdot (\mathbb{P}[U_a > 0] - \epsilon) \\ &= R \cdot ((1 - (1 - p_a)^U) - \epsilon), \end{aligned} \tag{27}$$

where $\mathbb{P}[U_a > 0] = 1 - (1 - p_a)^U$ represents the probability that at least one user is active during the slot.

C. OUTAGE PROBABILITY FOR SA VIA THE FBL APPROACH

We also analyze the system reliability in terms of the outage probability of a single transmission. We consider that the outage will happen if the overall SINR falls below a predetermined SINR threshold, denoted by γ_{th}.

For the system under consideration, and under the FBL regime with the selected code rate R, a predetermined γ_{th} threshold can be defined as a minimal value of the received SINR required to achieve a certain value of the error probability ϵ_{th}. Based on (23), the outage threshold can be determined as

$$\gamma_{th} = \Phi^{-1}(\epsilon_{th}), \tag{28}$$

where $\gamma = \Phi^{-1}(\epsilon)$ is obtained by inverting the expression in equation (23).

Considering the transmission from the reference user, the outage probability can be determined as

$$P_{out}(U_a) = \mathbb{P}\left[SINR < \gamma_{th} | U_a\right] = F_{SINR}\left(\gamma_{th} | U_a\right), \tag{29}$$

where $F_{SINR}(\gamma_{th}|U_a)$ is detailed in (18). The unconditional outage probability can be calculated as

$$P_{out} = \sum_{k=1}^{U} P_{out}(U_a = k)\, \mathbb{P}[U_a = k], \tag{30}$$

where $\mathbb{P}[U_a = k]$ was calculated in (26). Note that the reliability can be simply calculated as $P_R = 1 - P_{out}$.

D. SPECIAL CASE: SA WITHOUT CAPTURE IN THE FBL REGIME

The classical SA scheme without capture effect assumes that if more than one user is active in a given slot, a collision will happen and the packet is lost. Contrary to SA with capture, the classical SA receiver will only recover the packet if just one of the U IoT devices is active, i.e., $U_a = 1$. In that case, $\epsilon(U_a = k) = 0$ for $k > 1$, and thus the error probability is

$$\epsilon = \epsilon(U_a = 1)\, \mathbb{P}[U_a = 1], \tag{31}$$

where $\epsilon(U_a = 1)$ and $\mathbb{P}[U_a = 1]$ are determined by expressions (25) and (26), respectively, where $k = 1$.

TABLE 2. System parameters.

name	symbol	value
Transmitted optical power	P_t	30 mW
Photodetector surface area	A_r	1 cm^2
Responsivity	R_r	0.4 A/W
Optical filter gain	T_s	1
Refractive index of lens at a PD	ζ	1.5
FoV of receiver	Ψ	90°
Optical-to-electrical conversion efficiency	η	0.8
Noise power spectral density	N_0	10^{-21} W/Hz
System noise bandwidth	B	$B = 200$ kHz

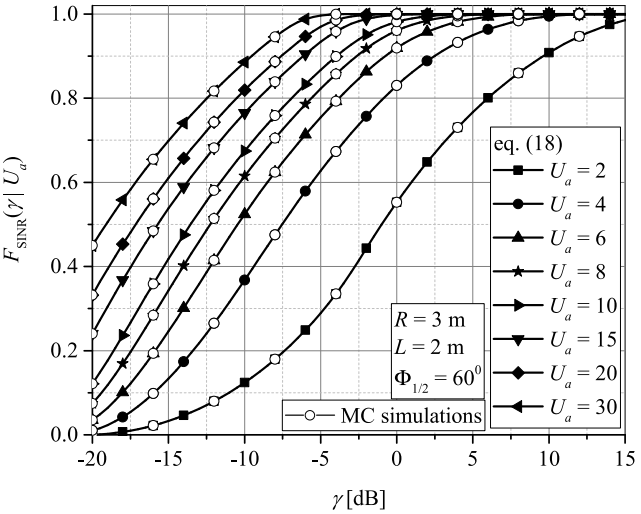

FIGURE 2. SINR CDF of the reference user conditioned on U_a, $F_{SINR}(\gamma_{th}|U_a)$.

Based on this, the throughput for SA without capture via the FBL approach can be defined as

$$\begin{aligned} T &= 0 \cdot \mathbb{P}[U_a = 0] + R \cdot (1 - \epsilon(U_a = 1)) \cdot \mathbb{P}[U_a = 1] \\ &\quad + \sum_{k=2}^{U} R \cdot (1 - \epsilon(U_a = k)) \cdot \mathbb{P}[U_a = k] \\ &= R \cdot (\mathbb{P}[U_a = 1] - \epsilon) \end{aligned} \tag{32}$$

since $\epsilon(U_a = k) = 0$ for $k > 1$.

The outage probability for the OWC system based on SA without capture in the FBL regime can be calculated as

$$P_{out} = P_{out}(U_a = 1)\, \mathbb{P}[U_a = 1] \tag{33}$$

since $P_{out}(U_a = k) = 0$ for $k > 1$.

Note that there will be no interference contribution under this scenario, since a packet can be decoded only if one user is active. According to this, for the error probability derivation in (24), the PDF given by (9) will be considered instead of the PDF $f_{SINR}(\gamma|U_a)$ derived in (17). Similarly, the outage probability will be derived based on the CDF given by (10) instead of the CDF of the SINR $F_{SINR}(\gamma|U_a)$ derived in (18).

V. NUMERICAL RESULTS AND DISCUSSION

In this section, using the analysis presented in Sec. III and Sec. IV, we focus on the design and performance evaluation

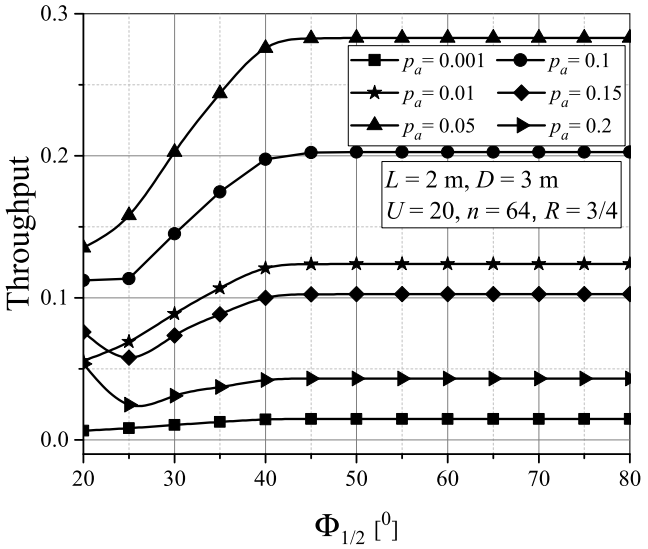

FIGURE 3. Throughput vs. $\Phi_{1/2}$ for different activation probability values p_a.

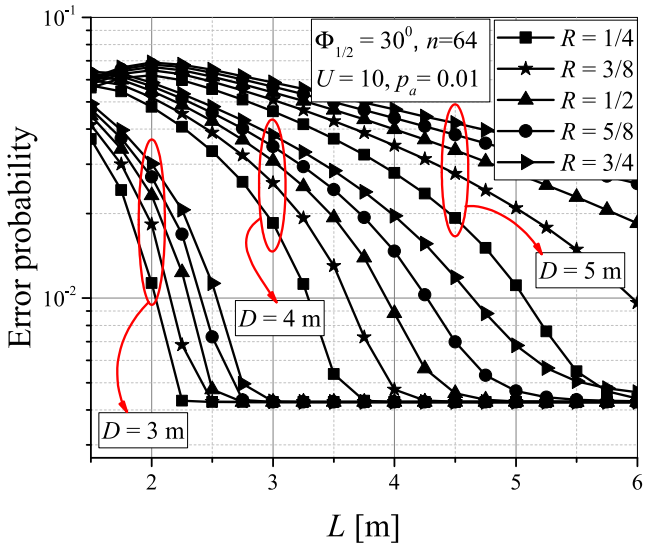

FIGURE 4. Error probability vs. L for different values of the rate R and the radius D.

of the proposed indoor OWC IoT system. The results are obtained by adopting the system parameters given in Table 1, which represent a typical situation in such environment. At the end of this section, we provide the overall throughput comparison of the proposed SA OWC IoT system with capture effect and the SA system without capture effect in the FBL regime. Further, since both the PDF and CDF of the *SINR* in (17) and (18), respectively, are given in integral form, the results are obtained by numerical computations performed through the FFT algorithm implemented in MATLAB.

Fig. 2 presents the CDF of the SINR derived in (18), comparing the results obtained by the numerical computations with the ones obtained via Monte Carlo (MC) simulations. These results match each other, validating the analysis performed in the previous section. In addition, a higher value of U_a, i.e., a greater number of active users, determines a stronger interference contribution. From Fig. 2 it can be noted that an increase in U_a leads to a situation in which the SINR progressively degrades, and consequently cause higher values of the CDF (and the outage probability).

Fig. 3 depicts the dependence of the throughput on the semi-angle at half illuminance $\Phi_{1/2}$, evaluated using the expression derived in (27), and considering different values of the activation probability p_a. An increase in p_a up to a certain value (i.e., $p_a = 0.05$ for the parameters in Fig. 3) results in a better performing system from the throughput point of view. However, after this value of p_a is surpassed, the throughput starts to decrease. In fact, it can be seen that there is an optimal value of p_a that maximizes the throughput performance of the system. On the other hand, depending on p_a (i.e., the number of active OWC-based IoT devices), a higher value of $\Phi_{1/2}$ may improve or degrade the system performance. The semi-angle at half illuminance of the LED determines the Lambertian order of the LED source, or, in other words, determines the received optical signal intensity from the active IoT users at the OWC AP. When the value of $\Phi_{1/2}$ is higher, the optical beam at the LED source output will be wider, thus the received power from the users that are not close to the AP will be higher. This holds for all IoT devices, thus the semi-angle will have a strong impact on both the reference user and the interference contributions (i.e., on the overall received SINR). To conclude, since $\Phi_{1/2}$ represents an important parameter which has a substantial impact on the received optical signal intensity, the number of active users (together with the overall interference) will determine if an increase in $\Phi_{1/2}$ leads to a higher or a lower system throughput.

Fig. 4 depicts the error probability of the considered OWC system in the FBL regime, as derived in (25), as a function of the OWC AP height L, for various levels of error protection parameterized by the code rate R. Additionally, three different values of radius D are considered. As expected, increasing R will result in an error protection performance deterioration. When the radius D is larger, the OWC IoT users will be distributed over a wider area, which will increase the chance that many of them are far distant from the OWC AP. Increasing the distance of the OWC users from the AP leads to a reduced received power, and consequently the overall SINR will be lower. This will affect the capture probability, and thus the error probability of the system will increase when D increases. Further, Fig. 4 shows that there is an error probability floor, which is reached for lower values of L as the radius D gets smaller. When the users are located in a wider area, the error floor appears at very high L. Note that the error probability floor is independent on the code rate R, as well as on the radius D. In other words, increasing the distance between the planes where the IoT users and the OWC AP are placed will not result in lower-error probability after the error floor is reached, for any value of D and R. Consequently,

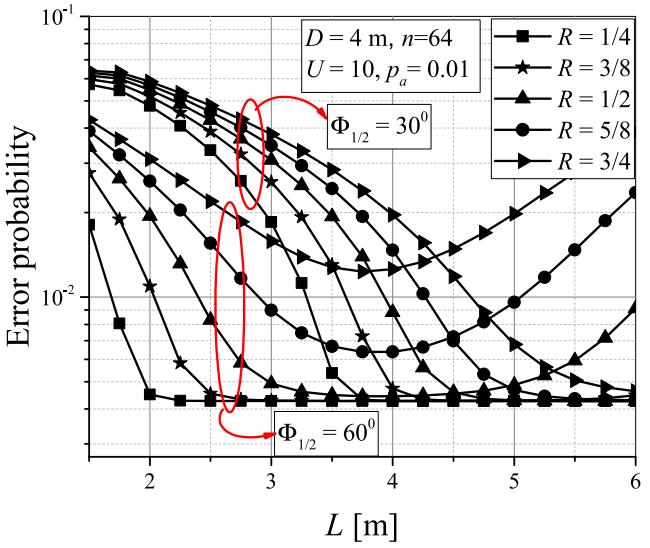

FIGURE 5. Error probability vs. L for different values of the rate R and the semi-angle $\Phi_{1/2}$.

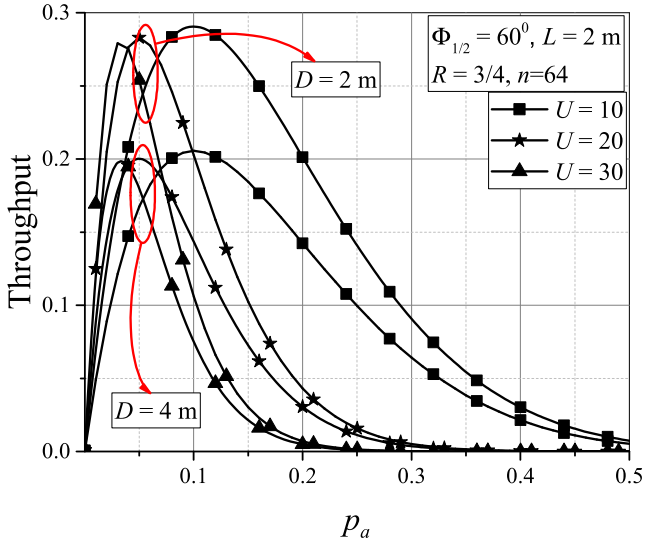

FIGURE 6. Throughput vs. p_a for different number of total IoT devices U.

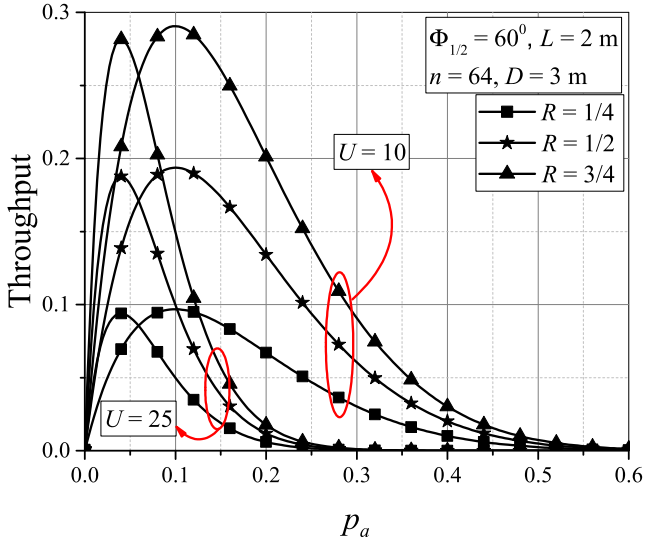

FIGURE 7. Throughput vs. p_a for different values of the maximum achievable rate R.

the geometric setup of the OWC based IoT framework has an impact on the system performance behavior in the FBL regime.

Fig. 5 presents the error probability ϵ of the considered OWC system under the FBL regime, derived in (25), as a function of the OWC AP height L, for different code rates R. In contrast to Fig. 4, the system behavior here is observed for two different values of the semi-angle at half illuminance $\Phi_{1/2}$. Similarly to Fig. 3, the system behaves differently when the value of $\Phi_{1/2}$ increases. For example, when $L < 3$ m, the error probability is lower for the larger semi-angle $\Phi_{1/2}$ value, whereas for $L > 5$ m, the system performance degrades sharply for higher values of $\Phi_{1/2}$. Additionally, a larger distance from the OWC IoT users to the AP (i.e., greater L) leads to a reduced received power, and to a lower overall SINR. This will affect the capture probability in such a way that larger L results in a behavior where the error probability of the considered system will initially decrease (eventually reaching the error probability floor in some cases), and, after some point that is dependent on $\Phi_{1/2}$, it will increase. Also, there is a minimum value of the error rate for different OWC setups, determined by the semi-angle $\Phi_{1/2}$ and the overall distance from the OWC IoT users to the AP. From Figs.4 and 5, it can be concluded that the effects of the rate value on the error probability performance is mainly dependent on the parameters L and $\Phi_{1/2}$.

Fig. 6 shows the dependence of the throughput derived in (27) on the activation probability p_a for different number of OWC-based IoT devices U and different values of radius D. As previously stated, a higher value of the radius D leads to a worse system performance, i.e., to a lower throughput level. A higher activation probability p_a and a higher number of total users U implies a higher number of active users in a slot. The number of active IoT devices determines the overall SINR, which has a direct impact on the potential of the capture effect. Consequently, as for the trend of each curve, it can be seen how, when the total number of users U in the system gets higher, the optimal value of p_a that maximizes T gets lower. Moreover, after achieving its maximum value, the system throughput starts decreasing with a further increase of p_a. Given a radius D, the maximum value of the throughput is rather insensitive with respect to the number of users. On the other hand, the optimal value of p_a that maximizes the throughput depends on the total number of users U, but, for fixed U it remains the same irrespective of the change in D. In conclusion, we can say that the geometric setup of the OWC based IoT system and the total number of users have a strong impact on the optimal system performance, and should be taken into consideration during the design of the access protocol.

In Fig. 7, we show the throughput derived in (27) as a function of the activation probability p_a for different values

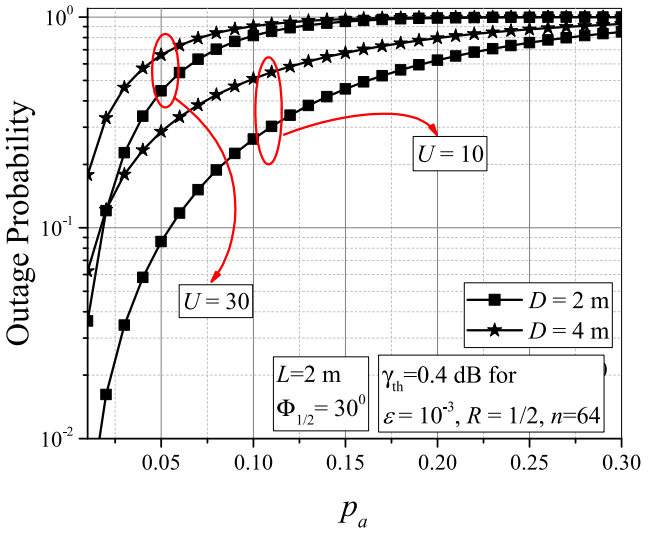

FIGURE 8. Outage probability vs. p_a for different values of the radius D and different number of users U.

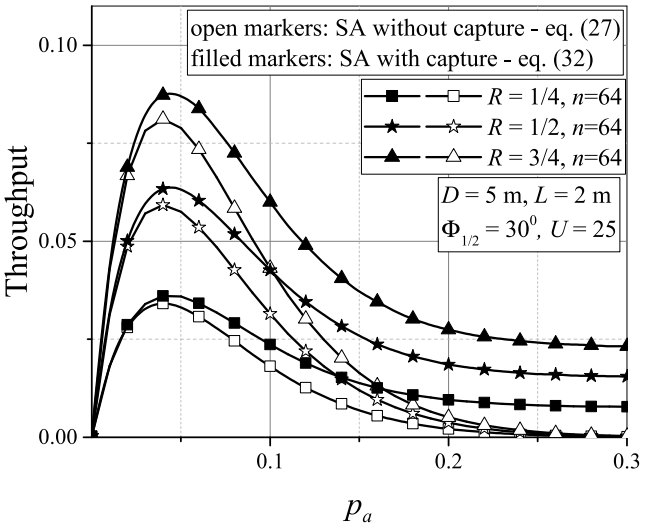

FIGURE 9. Comparisons of the throughput of the system with and without capture effect for different values of the rate R.

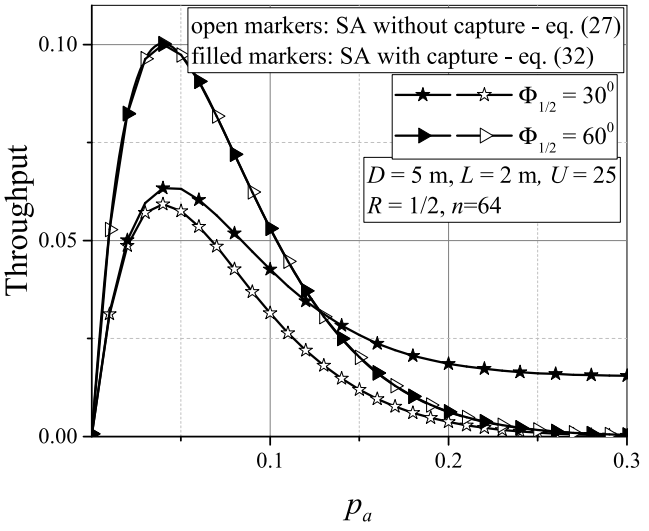

FIGURE 10. Comparisons of the throughput of the system with and without capture effect for different values of the semi-angle $\Phi_{1/2}$.

of the maximum achievable rate R. As previously stated, a higher rate corresponds to a degraded system performance. Moreover, Fig. 7 also reveals that there is an optimal value of p_a that leads to a maximum value of the system throughput. From the presented results, it can be concluded that the optimal value of p_a is different for a different number of overall users, but it is the same regardless of the employed rate R.

Based on the expression derived in (30), Fig. 8 depicts the outage probability dependence on the activation probability p_a, considering two values for the radius D ($D = 2$ m and $D = 4$ m). The outage threshold γ_{th} was defined in (28), and is obtained for an error probability of $\epsilon_{th} = 10^{-3}$, a rate $R = 1/2$ and a number of channel uses $n = 64$. As previously stated, a smaller value of the radius D results in a better system performance. As shown in the figure, a higher number of users lead to a system performance deterioration, since the interference contribution will be stronger. Furthermore, it can be noticed that the radius D and the total number of users U have an effect on the outage performance only for a smaller number of active users, while when $p_a > 0.25$ the radius D and the number of users U seem to have no impact on the outage probability. More precisely, the system outage will happen for $p_a > 0.3$, i.e., $P_{out} \approx 1$, for any D and U, since the overall SINR will not be higher than γ_{th} and the error probability target value $\epsilon_{th} = 10^{-3}$ will not be achieved.

Figs. 9 and 10 present the overall throughput comparison of the proposed SA OWC IoT system with capture (eq. (27)), and the SA system without capture effect (eq. (32)), in the FBL regime.

Fig. 9 shows the throughput dependence on p_a for various levels of error protection parameterized by the code rate R. A significant improvement in the system throughput is noticed in presence of the capture effect, especially for large code rates R. The results prove that the designed RA protocol represents an improvement from the point of view of the throughput, since the user data can be recovered even in presence of concurrent transmissions thanks to the successful exploitation of the capture effect.

Fig. 10 depicts the throughput dependence on p_a for two values of the semi-angle $\Phi_{1/2}$. The throughput improvement achieved by employing SA with capture is only evident for the lower semi-angle of $\Phi_{1/2} = 30^0$. As a contrast, the throughput remains the same when the semi-angle is higher, i.e., $\Phi_{1/2} = 60^0$. It can be concluded that the semi-angle of the OWC system plays a crucial role with respect to the interference contribution and its effects. More specifically, the capture effect leads to significant throughput improvement under the specific condition of limited interference (i.e. lower semi-angle), as may be expected.

In summary, we can conclude that the geometric setup (including the semi-angle at half illuminance $\Phi_{1/2}$, the radius

D and the height L), the number of active users U, and the code rate R play an important role in the possible maximization of the system performance. These parameters should be taken into account in order to appropriately design an access scheme for an OWC-based IoT system.

VI. CONCLUSION

In this paper, we have analyzed the uplink of an indoor OWC-based IoT system under the FBL regime and with a single AP. The system employs a SA-based access scheme, which exploits the capture effect, i.e., the possibility to decode user transmissions in the presence of interference from other users, which inherently exists in such setups. Based on the received SINR statistics, an analytical expression for the error probability in the FBL regime has been derived, as well as an expression for the overall throughput and the outage probability of the system under investigation. The derived expressions are used to obtain numerical results, which are further analyzed to assess the system performance behavior depending on the OWC framework and the channel model parameters.

The presented results have shown how the geometric setup of the OWC-based IoT system and the activation probability affect the error probability, the throughput and the outage probability performance. It has been proven that the OWC-based system geometry has a significant impact on the overall system performance, and should be taken into account during the design of any indoor OWC-based IoT system in order to assess and optimize the RA protocol performance. Our future work will include formulating and solving specific OWC-based IoT scenarios using optimisation methods that would provide optimal values of the system geometry parameters. Furthermore, we will work in the direction of establishment of a real world testbed, aiming to verify the effectiveness of presented analysis through the experimental results.

REFERENCES

[1] M. Z. Chowdhury, Md. T. Hossan, A. Islam, and Y. M. Jang, "A comparative survey of optical wireless technologies: Architectures and applications," *IEEE Access*, vol. 6, pp. 9819–9840, 2018.

[2] Z. Ghassemlooy, W. Popoola, and S. Rajbhandari, *Optical Wireless Communications: System and Channel Modelling With MATLAB*. Boca Raton, FL, USA: CRC Press, 2013.

[3] Z. Ghassemlooy, L. N. Alves, S. Zvanovec, and M. A. Khalighi, *Visible Light Communications: Theory and Applications*. Boca Raton, FL, USA: CRC Press, 2017.

[4] Z. Ghassemlooy, S. Arnon, M. Uysal, Z. Xu, and J. Cheng, "Emerging optical wireless communications-advances and challenges," *IEEE J. Sel. Areas Commun.*, vol. 33, no. 9, pp. 1738–1749, Sep. 2015.

[5] P. Popovski, *Wireless Connectivity: An Intuitive and Fundamental Guide*. Hoboken, NJ, USA: Wiley, 2020.

[6] M. Berioli, G. Cocco, G. Liva, and A. Munari, "Modern random access protocols," *Found. Trends Netw.*, vol. 10, no. 4, pp. 317–446, 2016.

[7] R. Rom and M. Sidi, *Multiple Access Protocols: Performance and Analysis*. Springer, 2012.

[8] F. Clazzer, A. Munari, G. Liva, F. Lazaro, C. Stefanovic, and P. Popovski, "From 5G to 6G: Has the time for modern random access come?" in *Proc. 1st 6G Summit*, Levi, Finland, Mar. 2019, pp. 1–2.

[9] L. G. Roberts, "ALOHA packet system with and without slots and capture," *ACM SIGCOMM Comput. Commun. Rev.*, vol. 5, no. 2, pp. 28–42, Apr. 1975.

[10] A. Munari, F. Clazzer, G. Liva, and M. Heindlmaier, "Multiple-relay slotted ALOHA: Performance analysis and bounds," *IEEE Trans. Commun.*, vol. 69, no. 3, pp. 1578–1594, Mar. 2021.

[11] W. S. Jeon, S. B. Seo, and D. G. Jeong, "POMDP-based contention resolution for framed slotted-ALOHA protocol in machine-type communications," *IEEE Internet Things J.*, vol. 9, no. 15, pp. 13511–13523, Aug. 2022.

[12] J. F. Grybosi, J. L. Rebelatto, and G. L. Moritz, "Age of information of SIC-aided massive IoT networks with random access," *IEEE Internet Things J.*, vol. 9, no. 1, pp. 662–670, Jan. 2022.

[13] M. Zorzi, "Mobile radio slotted ALOHA with capture, diversity and retransmission control in the presence of shadowing," *Wireless Netw.*, vol. 4, no. 5, pp. 379–388, 1998.

[14] M. S. Corson and A. Ephremides, "An analysis of multi-receiver, non-adaptive, slotted ALOHA with capture for wireless communications in factories," in *Proc. IEEE INFOCOM*, San Francisco, CA, USA, Mar. 1993, pp. 421–428.

[15] Y. Onozato, J. Liu, and S. Noguchi, "Stability of a slotted ALOHA system with capture effect," *IEEE Trans. Veh. Technol.*, vol. 38, no. 1, pp. 31–36, Feb. 1989.

[16] A. Gupta and X. Fernando, "Exploring secure visible light communication in next-generation (6G) Internet-of-Things," in *Proc. Int. Wireless Commun. Mobile Comput. (IWCMC)*, Jun. 2021, pp. 2090–2097.

[17] S. S. Oyewobi, K. Djouani, and A. M. Kurien, "Visible light communications for Internet of Things: Prospects and approaches, challenges, solutions and future directions," *Technologies*, vol. 10, no. 1, p. 28, Feb. 2022.

[18] M. Z. Chowdhury, M. Shahjalal, M. K. Hasan, and Y. M. Jang, "The role of optical wireless communication technologies in 5G/6G and IoT solutions: Prospects, directions, and challenges," *Appl. Sci.*, vol. 9, no. 20, p. 4367, Oct. 2019.

[19] A. Hamza and T. Tripp, "Optical wireless communication for the Internet of Things: Advances, challenges, and opportunities," *TechRxiv*, Jul. 2020.

[20] M. Haus, A. Y. Ding, Q. Wang, J. Toivonen, L. Tonetto, S. Tarkoma, and J. Ott, "Enhancing indoor IoT communication with visible light and ultrasound," in *Proc. IEEE Int. Conf. Commun. (ICC)*, May 2019, pp. 1–6.

[21] S. R. Teli, S. Zvanovec, and Z. Ghassemlooy, "Optical Internet of Things within 5G: Applications and challenges," in *Proc. IEEE Int. Conf. Internet Things Intell. Syst. (IOTAIS)*, Bali, Indonesia, Nov. 2018, pp. 40–45.

[22] C.-W. Chen, W. C. Wang, J. T. Wu, H. Y. Chen, K. Liang, L. Y. Wei, Y. Hsu, C. W. Hsu, C. W. Chow, C. H. Yeh, and Y. Liu, "Visible light communications for the implementation of Internet-of-Things," *Opt. Eng.*, vol. 55, no. 6, 2016, Art. no. 060501.

[23] Z. Wu, M. Ismail, E. Serpedin, and J. Wang, "Data-driven link assignment with QoS guarantee in mobile RF-optical HetNet of things," *IEEE Internet Things J.*, vol. 7, no. 6, pp. 5088–5102, Jun. 2020.

[24] A. Celik, I. Romdhane, G. Kaddoum, and A. M. Eltawil, "A top-down survey on optical wireless communications for the Internet of Things," *IEEE Commun. Surveys Tuts.*, vol. 25, no. 1, pp. 1–45, 1st Quart., 2023.

[25] D. Vukobratovic and F. J. Escribano, "Adaptive multi-receiver coded slotted ALOHA for indoor optical wireless communications," *IEEE Commun. Lett.*, vol. 24, no. 6, pp. 1308–1312, Jun. 2020.

[26] L. Zhao, X. Chi, and W. Shi, "A QoS-driven random access algorithm for MPR-capable VLC system," *IEEE Commun. Lett.*, vol. 20, no. 6, pp. 1239–1242, Jun. 2016.

[27] L. Zhao, X. Chi, and S. Yang, "Optimal ALOHA-like random access with heterogeneous QoS guarantees for multi-packet reception aided visible light communications," *IEEE Trans. Wireless Commun.*, vol. 15, no. 11, pp. 7872–7884, Nov. 2016.

[28] T. Li, X. Chi, F. Ji, H. Shi, and S. Wang, "Optimal optical camera communication-ALOHA random access algorithm aided visible light communication system," *Opt. Eng.*, vol. 59, no. 7, p. 1, Jul. 2020.

[29] Y. Polyanskiy, H. V. Poor, and S. Verdu, "Channel coding rate in the finite blocklength regime," *IEEE Trans. Inf. Theory*, vol. 56, no. 5, pp. 2307–2359, May 2010.

[30] M. Petkovic, T. Devaja, D. Vukobratovic, F. J. Escribano, and C. Stefanovic, "Reliability analysis of slotted ALOHA with capture for an OWC-based IoT system," in *Proc. 17th Int. Symp. Wireless Commun. Syst. (ISWCS)*, Sep. 2021, pp. 1–6.

[31] K. Wang, T. Song, Y. Wang, C. Fang, J. He, A. Nirmalathas, C. Lim, E. Wong, and S. Kandeepan, "Evolution of short-range optical wireless communications," *J. Light. Technol.*, vol. 41, no. 4, pp. 1019–1040, Feb. 15, 2023.

[32] J. M. Kahn and J. R. Barry, "Wireless infrared communications," *Proc. IEEE*, vol. 85, no. 2, pp. 265–298, Feb. 1997.
[33] M. Petkovic, D. Vukobratovic, A. Munari, and F. Clazzer, "Relay-aided slotted ALOHA for optical wireless communications," in *Proc. 12th Int. Symp. Commun. Syst., Netw. Digit. Signal Process. (CSNDSP)*, Jul. 2020, pp. 1–6.
[34] A. Papoulis and H. Saunders, *Probability, Random Variables and Stochastic Processes*, 4th ed. New York, NY, USA: McGraw-Hill, 2002.
[35] I. S. Gradshteyn and I. M. Ryzhik, *Table of Integrals, Series, and Products*. 6th ed. New York, NY, USA: Academic, 2000.
[36] J. H. Curtiss, "On the distribution of the quotient of two chance variables," *Ann. Math. Statist.*, vol. 12, no. 4, pp. 409–421, Dec. 1941.
[37] G. Durisi, T. Koch, and P. Popovski, "Towards massive, ultra-reliable, and low-latency wireless communication with short packets," *Proc. IEEE*, vol. 104, no. 9, pp. 1711–1726, Sep. 2016.
[38] N. Hesham, J. Hossain, and A. Chaaban, "Transmission rate analysis for large scale uplink networks in the finite block-length regime," in *Proc. IEEE Wireless Commun. Netw. Conf. (WCNC)*, Glasgow, U.K., Mar. 2023, pp. 1–6.
[39] J. Scarlett, V. Y. F. Tan, and G. Durisi, "The dispersion of nearest-neighbor decoding for additive non-Gaussian channels," *IEEE Trans. Inf. Theory*, vol. 63, no. 1, pp. 81–92, Jan. 2017.
[40] J. Park, "Rate analysis of ultra-reliable low-latency communications in random wireless networks," 2019, *arXiv:1910.13868*.

TIJANA DEVAJA (Graduate Student Member, IEEE) received the M.Sc. degree in electrical engineering from the Faculty of Technical Sciences, University of Novi Sad, Novi Sad, Serbia, in 2017. She is currently pursuing the Ph.D. degree in wireless communication systems with the Faculty of Technical Sciences. Her research interests include communication theory, wireless communication systems, and information theory.

MILICA PETKOVIĆ (Member, IEEE) received the M.Sc. and Ph.D. degrees in electrical engineering from the Faculty of Electronic Engineering, University of Nis, Serbia, in 2010 and 2016, respectively. Currently, she is an Assistant Professor with the Faculty of Technical Science, University of Novi Sad, Serbia. Her research interests include digital communications systems and signal processing, with an emphasis on optical wireless communications.

FRANCISCO J. ESCRIBANO (Senior Member, IEEE) received the degree in telecommunications engineering from ETSIT-UPM, Spain, and the Ph.D. degree from Universidad Rey Juan Carlos, Spain. He is currently an Associate Professor with the Department of Signal Theory & Communications, Universidad de Alcalá, Spain, where he is involved in several undergraduate and master's courses in telecommunications engineering. He has been a Visiting Researcher with Politectnico di Torino, Italy, and EPFL, Switzerland. His research interests include communications systems and information theory, mainly on the topics of channel coding, modulation and multiple access, and on the applications of chaos in engineering.

ČEDOMIR STEFANOVIĆ (Senior Member, IEEE) received the Diploma (Ing.), Mr.-Ing., and Ph.D. degrees from the University of Novi Sad, Serbia. He is currently a Full Professor with the Department of Electronic Systems, Aalborg University, where he leads a research group on edge computing and networking. He is also a Project Coordinator of the ITN Project WindMill and a Principal Researcher on Horizon RIA Project Sixthsense, Horizon Twinning Project INCOMING, and Independent Research Fund Denmark (DFF) Project CLIMB. He has coauthored more than 120 peer-reviewed publications. His research interests include communication theory and wireless communications and he specializes in the IoT, 5G/beyond 5G, and mission-critical communications. He serves as an Editor for the IEEE Internet of Things Journal.

DEJAN VUKOBRATOVIĆ (Senior Member, IEEE) received the Ph.D. degree in electrical engineering from the University of Novi Sad, Serbia, in 2008. From 2009 to 2010, he was a Marie Curie Intra-European Fellow with the University of Strathclyde, Glasgow, U.K. Since 2019, he has been a Full Professor with the Department of Power, Electronics and Communication Engineering, University of Novi Sad. His research interests include wireless communication systems and the Internet of Things.